Challenge Journal of Structural Mechanics

Research Article

Assessment of an old roadway bridge under static and seismic loading conditions

Mehmet Fatih Yılmaz [a], Abdulkadir Cüneyt Aydın [b,*]

[a] *Department of Civil Engineering, Ondokuz Mayıs University, 55139 Samsun, Turkey*
[b] *Department of Civil Engineering, Atatürk University, 25240 Erzurum, Turkey*

ABSTRACT

A large proportion of road and railway bridges, present in Turkey served for many years, have been completed their service life or will soon. Continuing safety and sustainability of these bridges under traffic loads have been of great increasing importance to roadway and railway transportation line to be continuous servicing. In addition, the demolition and reconstruction of bridges that have reached the end of their service life or are nearing completion will have a negative impact on the country's economy. All of these requirements' detailed examination of bridges in order to provide economical and safe service, considering current vehicle loads and earthquake loads. The Mahmutçavuş Bridge is investigated as a simply supported continuous composite roadway bridge at this work. The finite-element model of the bridge is constituted by site investigation and measurement. Different truckloads using for the design of the bridge are determined, and static analysis of the bridge is conducted. Seven earthquake records are scaled for two different earthquake design spectrums. The nonlinear time-history analyses are conducted, considering Δ-δ effects. The performance of the bridge for varying truckloads and earthquake loads is investigated, and results are discussed in detail.

ARTICLE INFO

Article history:
Received 3 December 2020
Revised 20 January 2021
Accepted 2 March 2021

Keywords:
Roadway bridge
Steel composite bridge
Time-history analysis
Pushover analysis

1. Introduction

Turkey has in the past experienced major earthquakes and, consequently, significant structural, life, and property losses (Damci et al., 2015; Inel et al., 2008; Korkmaz et al., 2010; Tolon and Mızrak, 2017). The disasters in the past have shown that timely delivery to the exposure areas is important as the damage occurs to the structure, and many urgent intervention plans are prepared for quick implementation in the area. Highway lines are the most basic transportation network used in transportation to disaster areas. For this reason, the fact that road transport systems continue to be functional after natural disasters are of great importance in order that disaster areas can be reached quickly and that necessary intervention can be made on time. Bridges are the vulnerable components of the transportation system, and due to economic reasons, the existing system needs to be used as long as possible, and its safety is ensured. The long service life and increasing traffic load require more detailed investigation on the roadway bridge to sustain the safe and economical servicing of the road.

Erzurum Province includes many active seismic faults and has been exposed to devastating earthquakes in the near past; Horasan-Narman 1983 (Ms=6.8), Erzurum 1859, Erzurum 1901 (MS=6.1), Horasan 1924 (Ms=6.8), Hinis (Erzurum) 1952 (Ms=5.6), Horasan-Narman 1983 (Ms=6.7), Balkaya 2984 (Mb=6.4), Şenkaya 1999 (MI=5.1), Aşkale 2004 (Ms=5.3). Because of these major earthquakes, much loss of life and property was experienced. In order to prevent loss of life and property, the earthquake performance of existing structures and bridges in the Erzurum region should be determined. Past earthquakes show that bridges are vulnerable components of the roadway system with regard to seismic

* *Corresponding author*. Tel.: +90-442-231-4781 ; Fax: +90-442-231-4910 ; E-mail address: acaydin@atauni.edu.tr (A. C. Aydın)
ISSN: 2149-8024 / DOI: https://doi.org/10.20528/cjsmec.2021.02.006

damage, and the main reason for damage in steel bridges essentially originates from buckling, extremely low-cycle fatigue, tension, shearing break, and damage to supports (Usami and Ge, 2009; Rokneddin et al., 2014). Past design criteria for roadway bridges do not include seismic load, and with an increase in vehicle loads, questions are starting to be asked regarding whether or not the performance of old roadway bridges is sufficient and safe. Also, bridges lose design load-carrying capacity due to many different aging phenomena, such as corrosion of steel bridge components, which is one of the well-known deterioration processes seen on bridges, and damage occurring after natural hazards (Ghosh and Padgett, 2010). Because of the deterioration of bridges and design that does not consider seismic code, the bridges are vulnerable to seismic events, and many different retrofitting methods are updated and used to increase the safety of these bridges (Usami et al., 2005). Besides, the Economical design of bridges for different truckloads and different beam configurations was investigated, which is essential for the financial growth of the civilization (Atmaca, 2019).

The seismic performance of bridges is determined using a mathematical model of the bridge. There are three analytical methods used for the seismic assessment of bridges: Static analysis, pushover analysis, and time history analysis. Static analysis is essentially used to calculate the live load acting on the bridge and increase the traffic load with a constant to determine the dynamic effect of the load and apply seismic load as a lateral static load and equivalent earthquake load method and mod shape assembly method. Pushover analysis and time history analysis are conducted to determine the seismic performance of the bridge. Pushover analysis applies a fundamental modal load to the bridge system and increases the load until a target displacement or collapse of the bridge and gives conservative results (Lu et al., 2004; Zheng et al., 2003). Time history analysis (THA) gives more realistic results but requires more time and computational efforts. However, with advances in computer technology, THA is beginning to be used in seismic assessment of structures and bridge systems (DesRoches et al., 2004; Nielson and DesRoches, 2007; Padgett and DesRoches, 2008; Saadeghvaziri and Yazdani-Motlagh, 2008). In addition to lateral seismic force, vertical seismic force is also critical to determine the seismic performance of the bridge, and recent seismic code has started to consider vertical ground motion in bridge design (Kunnath et al., 2008).

These studies investigate an existing bridge that was serviced until 1961. A finite element model using site investigation and finite element model is constituted. A different truckload is applied to the model to determine the highest moment occurring in the superstructure and the maximum displacement in the span. Seven seismic records are used for time history analysis with matching spectral response acceleration for 2% and 10% acceding probability for a 50-year period. Damage in the bridge column, steel girders, and bridge bearings are investigated. Location and progress of damages are determined according to the pushover-analysis. The weakest component of the bridge is determined according to the time history analysis. Spectral acceleration of scaled earthquake records shows that the record has different acceleration values for higher frequency from the 475-year design spectrum but closer values for the 2475-year design spectrum. Bridge components performance is determined considering both earthquake scenarios.

2. Description of the Bridge

Mahmutçavuş Bridge is located 400 km from Pasinler, Oltu, Narman National roadway, on the Kışla village roadway. The bridge is a typical multi-span continuous steel roadway bridge. The first and last spans of the bridge are 10 m long, and the middle span of the bridge is 12 m long. The total length of the bridge is 56 meters, and the total width of the bride is 5.4 meters. The bridge is in service since its construction time in 1961. There are two gravity abutments and four steel piers on which the superstructure is positioned. A composite steel section and concrete slabs are used to constitute the superstructure of the bridge, while elastomeric fixed bearings are positioned at the middle piers, and elastomeric expansion bearings are positioned at the abutments. The piers of the bridge are constituted by welding two IPN240 steel sections, and each pier is composed of four columns. The width of the bend beam is 52 cm, and the height of the bend beam is 58 cm. Fig. 1 shows the general view of the bridge, and Fig. 2 shows the section view of the bridge. The superstructure of the bridge is composed of 5 IPN360 steel beams and concrete slabs. The bridge overpasses the Norman stream, and the water height of the river changes seasonally. In winter, only one pier of the bridge is underwater, but in spring and summer, all piers of the bridge are exposed to water. The total height of the bridge piers is 4m, but because of soil accumulation in the river, half of the columns are placed under accumulated soil.

3. Finite Element Model

A finite element model of the bridge is constituted by Sap2000 finite element software according to site investigation and measurement. Because of the construction date of the bridge, there is no available shop drawing and design project. Therefore, all sections and distances are measured on-site, and the finite element models of the bridge are constituted. Two node beam elements are used to model the piers, and the superstructure and 4-node shell elements are used to model the concrete slab. The supports are modeled using nonlinear link elements. The friction coefficient between the bearings and supports are calculated as for elastomeric pads and modeled with a friction link. Fig. 3 shows a 3D finite element model of the bridge, Fig. 4 shows the actual photograph of the bridge, and Fig. 5 shows the hysteresis model of fixed and elastomeric expansion bearings.

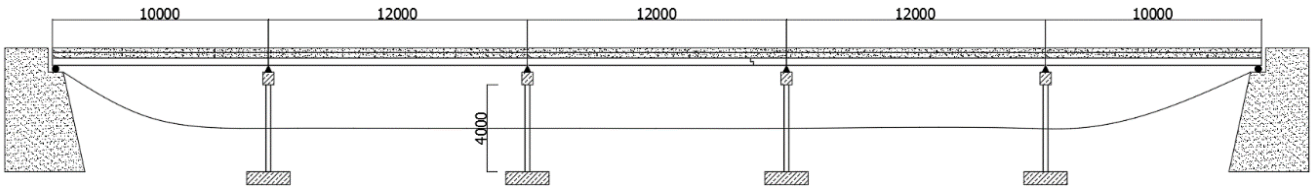

Fig. 1. General view of MSC composite bridge.

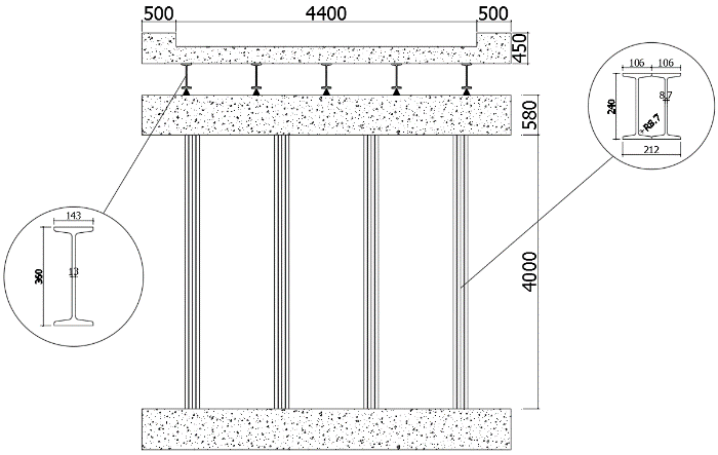

Fig. 2. Section view of MSC composite bridge.

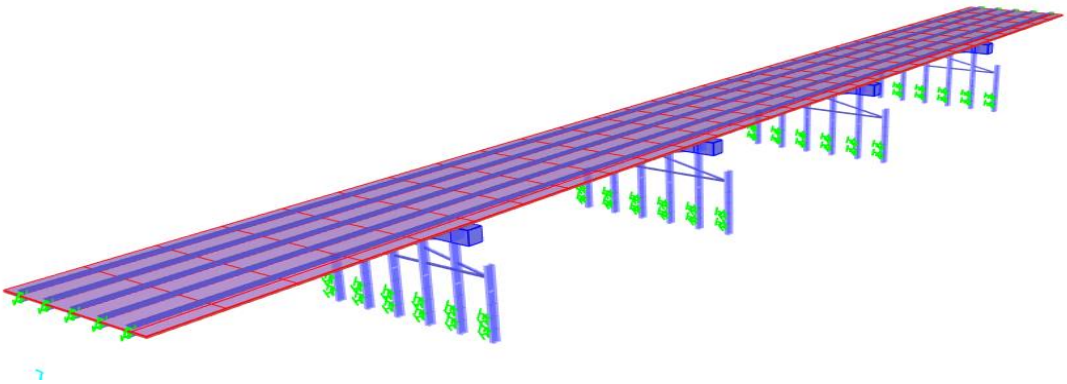

Fig. 3. 3D finite element view of MSC steel roadway bridge.

Fig. 4. Photograph of the bridge.

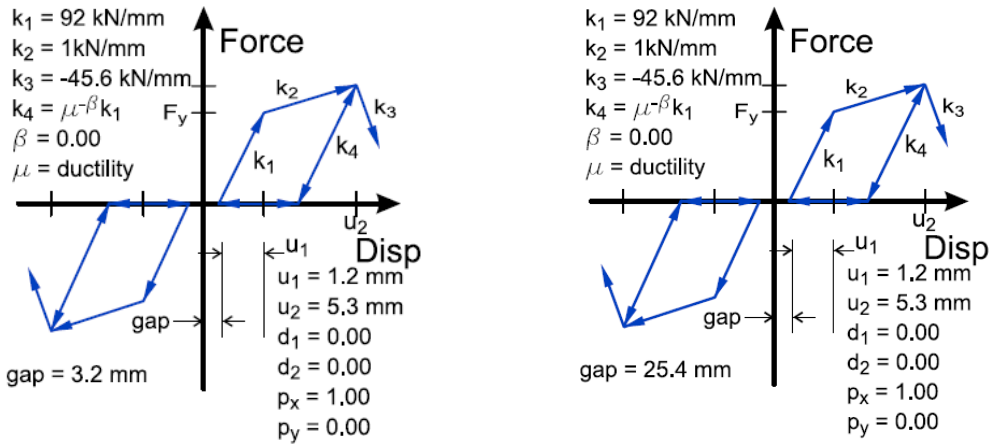

Fig. 5. Hysteresis models of: a) Fixed elastomeric bearing; b) Expansion elastomeric bearing (Nielson, 2005).

Since there is no specimen test for these MSC bridges, the material properties are obtained from previous studies in the literature. Yields and ultimate strengths are given for European railway and roadway bridges and are considered as MPa and MPa, respectively (Larsson and Lagerqvist, 2009). Both material and geometric nonlinear behaviors of bridges are considered in this study.

To conduct nonlinear time history analysis and push-over analysis, a finite element model of the bridge is constituted using Seismostruct finite element software. Material nonlinearity is defined by nonlinear hysteretic material modeling (Fig. 6) and the spread fiber model. Geometric nonlinearity is considered as *P*-Δ large displacement. Modal properties for the Mahmutçavuş Bridge are illustrated in Table 1. The first mod of the bridge is an effective mod and represents 55% of the longitudinal mass. The second, third, and fourth modes constitute transverse mods, which represent 82% of the bridge transverse mass and the periods of these mods change between 0.27s to 0.33s. The dominant vertical mod is also calculated. The modal participation mass ratio for the dominant vertical mod is 0.44, and the period is 0.098s.

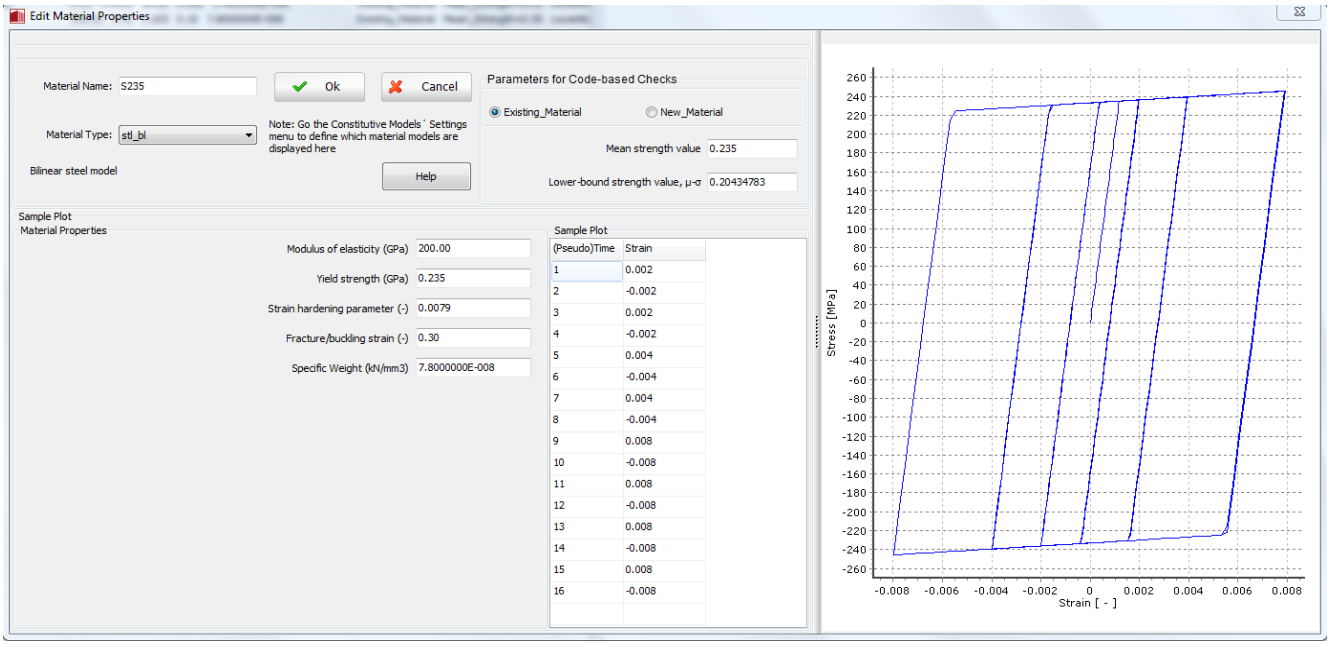

Fig. 6. Hysteretic steel material model.

Table 1. Modal properties for MSC steel girder bridge.

Mode Number	Period	Longitudinal	Transverse	Vertical
First	0.4937	0.5487	0	0
Second	0.3336	0	0.4023	0
Third	0.2930	0	0.1058	0
Fourth	0.2759	0	0.3119	0
Twelfth	0.0987	0	0	0.4432

4. Loading of the Bridge

Mahmutçavuş Bridge is designed with H15-44 truckload, as illustrated in Fig. 7. In AASHTO (1935) specification, there are H15-44, H20-44, HS15-44, and HS20-44 truckloads used in the design of the bridge, considering the weight of the truck. In addition to this truckload, 9.35kN/m (240 flp), the continuous load is applied to the structure as mentioned in AASHTO (1935). The one-line truckload is applied to two longitudinal steel girders, and maximum displacement, maximum positive moment, and maximum negative moment are recorded as a result of static analysis.

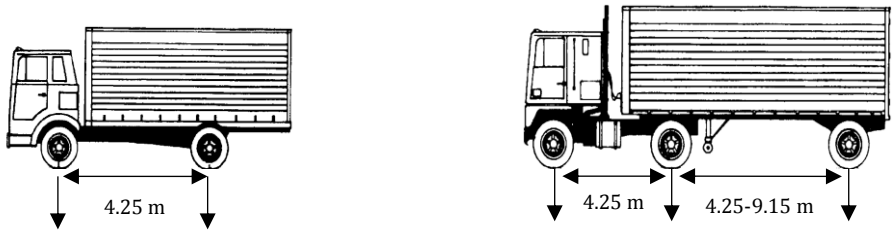

H15-44	30 kN	120 kN	HS15-44	30 kN	120 kN	120 kN
H20-44	40 kN	160 kN	HS20-44	40 kN	160 kN	160 kN

Fig. 7. Design truck load (HL-93, Caltrans).

AASHTO also developed an impact factor to increase the live load to account for the bounce and sway of vehicles, and the formulation is shown in Eq. (1). L is the length of the bridge span in feet.

$$I = \frac{50}{L+125} \leq 0.3 \quad (1)$$

Using Eq. (1), the impact factor for 10m span and 12m span is calculated as 0.31 and 0.30, respectively. According to these calculations, the live load needs to be increased by 30%.

Maximum displacement and moments calculated in the bridge span under truckload are illustrated in Table 2. According to AASHTO specifications, the maximum permitted displacement is 15mm (L/800). The calculated vertical displacement in the bridge span changes between 29.06 mm and 41.89 mm and does not satisfy the specification limits. The maximum positive moment in the steel girder changes between 107.93 kN/m and 149.105 kN/m, and the minimum moment in the steel girder bridge changes between -118.47 kN/m and -176.22 kN/m. According to these moments, the maximum compression and tension stress in the steel girder beam change between 118.67 N/mm^2 and 193.75 N/mm^2. The examined stress is very close to the steel yielding stress limits. To the safety of the bridge transportation, detailed measurement and investigation should be done, and the serves load of the bridge should be limited before these measurement and further repair activities.

Table 2. Maximum displacement and moment calculated on the bridge span.

	Max Displacement (mm)	Max Moment (kN/m)	Min Moment (kN/m)
H15-44	34.30	139.03	-176.22
H20-44	41.89	149.105	-173.61
HS15-44	29.06	107.93	-118.47
HS20-44	35.10	128.48	-146.38

5. Pushover Analysis of the Bridge

Static pushover analysis in the transverse direction is conducted to determine the nonlinear behavior of the bridge. Lateral loads are applied to the bridge superstructure. Material nonlinearity is modeled with a spread fiber plastic hinge. Nonlinear material is modeled using a bilinear steel model. Geometric nonlinearity is considered with Δ-δ large displacement. Transverse displacement limits are assumed to be 20% off pier height, and the structure is pushed at the displacement limits. Fig. 8 shows the pushover curve and plastic hinge occurring in the bridge.

When the peak displacement reaches 16mm, the first plastic hinges occur at the brace member. When the peak displacement reaches 32 mm, the plastic hinge of the second and third bridge piers began to occur in the areas where the soil came into contact with the piers. As the horizontal displacement increases further, the plastic hinges are formed at the upper ends of the bridge piers and in the regions where the brace connects to the bridge piers. In the idealized force-displacement diagram in Fig. 8, the yielding displacement of the bridge is calculated as 38.13mm with 3380 kN base shear. For two types of design spectrums: level 1

(2% exceedance possibility for 50 years) and level 2 (10% exceedance possibility for 50 years), target displacements are calculated as 45.36mm and 22.79 mm, respectively. The bridge is pushed until the top displacement reaches 800mm, and the deform shape of the bridge is shown in Fig. 9. Using the deform shape of the bridge, lateral displacement at the top of all piers can easily be calculated.

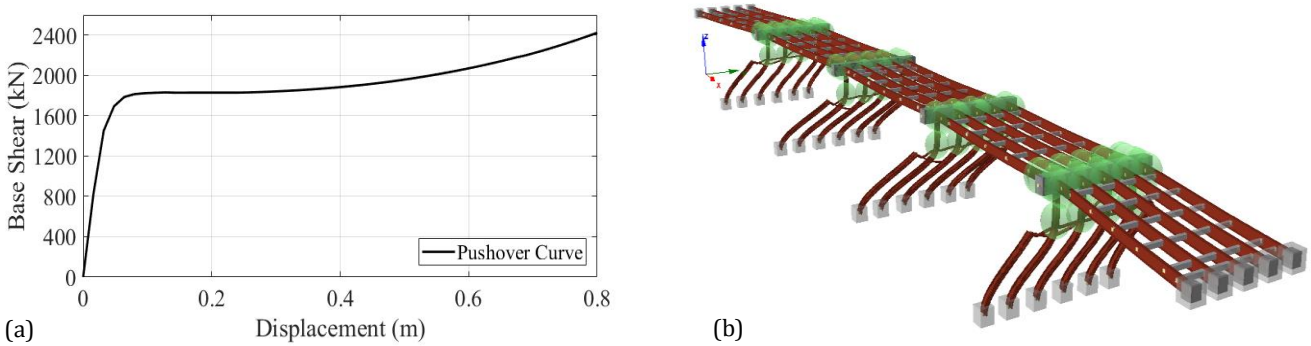

Fig. 8. Pushover analysis of Mahmutçavuş Bridge:
a) Pushover curve; b) 3D view of the location of the plastic hinges on the bridge.

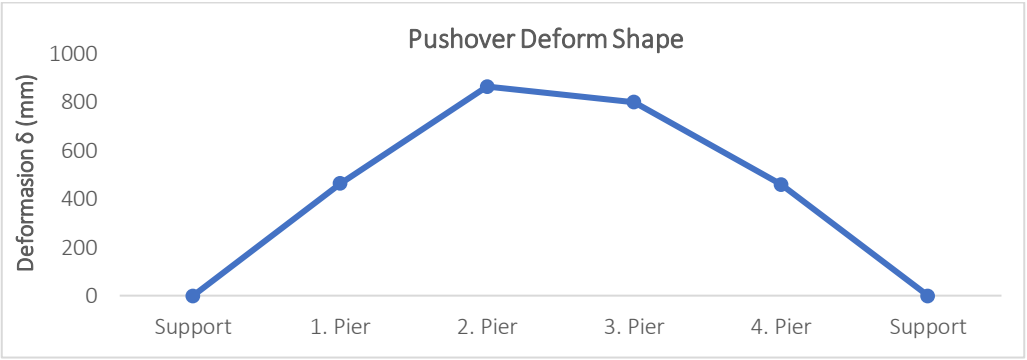

Fig. 9. Deform shape of the bridge under pushover analysis.

6. Time-History Analysis of the Bridge

Erzurum is located in a seismically active area of Turkey, and many catastrophic seismic events have occurred. 1901, Erzurum (Ms=6.1), 1924 Horasan (Ms=6.8), 1983, Horasan-Narman (Ms=6.8), 1984, Balkaya (Erzurum) (Ms=6.4) earthquakes are some of the devastating seismic events that have occurred in Erzurum Province. The investigated MSC bridge is located at the coordinates of 400, 20', 28" N, and 410,54', 56" E. According to Turkish Seismic Risk Maps, short-period spectral acceleration (S_(a_0.2s)) and long-period spectral acceleration (S_(a_1.0s)) values are obtained as 0.718g and 0.181g for 10% existing possibility for 50 years and 1.368g and 0.340g for 2% existing possibility for 50 years respectively.

Seven different strike-slip earthquake records are selected from Erzurum and other seismic areas and scaled to a design spectrum specified in the Turkish seismic risk maps for bridge location. The scaling of the earthquake records was made so that the scaled earthquake acceleration was not smaller than the design spectral acceleration, between 0.2 and 1.5 times the dominant period of the bridge. Fig. 10 shows the scaled earthquake record for a 475-year return period, and Fig. 11 shows the spectral acceleration of matched earthquake data and design spectrum for 475-year and 2475-year return periods.

6.1. Damage limit states

In determining the earthquake performance of the bridges, two different earthquake loads were defined: light earthquake (LL) and strong earthquake (UL). The LL earthquake is the earthquake with a high probability of being encountered during the lifetime of the bridge, and although the earthquake load of UL is greater than LL, the earthquake load is less likely to be encountered during the lifetime of the bridge. Damage occurs after extreme events described in the literature with a damage level of bridge elements is categorized into four different classes in the literature. These classes are slight damage, moderate damage, extensive damage, and collapse. In the bridge design, it is aimed to design it in such a way that slight damage could be visualized under LL earthquake to be exposed during the lifetime of the bridge, and bridges could be continuous servicing. Under UL earthquake load, bridges are expected to sustain life safety (extensive damage) damage level, and no collapse phenomena are expected under UL earthquake load.

An important part of the bridge was designed without considering seismic load. As a result, different damage to the bridge under seismic events has been seen. Deficiency of column rotation capacities and shear capacities and damage to bridge bearings and steel braces were

seen in the 1978 Miyagi-ken-oki and 2011 Great East Japan earthquakes (Kawashima, 2012). Damage to steel columns, lateral braces, and bearings have also been seen in different earthquake events. Bridges exposed to earthquakes allow engineers to observe bridge performances under real conditions. In light of the data obtained from past earthquakes and experimental studies, many different damage limit states have been identified in the literature for the determination of bridge performance (Table 3) (Bruneau et al., 1996; Bruneau, 1998).

In this study, rotation limits were used to determine the four types of damage in the columns (see Table 3), and the four displacement limits determined for bearing damage are shown in Table 4. Also, yielding and fracture strain limits are used to determine the damage limit state of steel brace members.

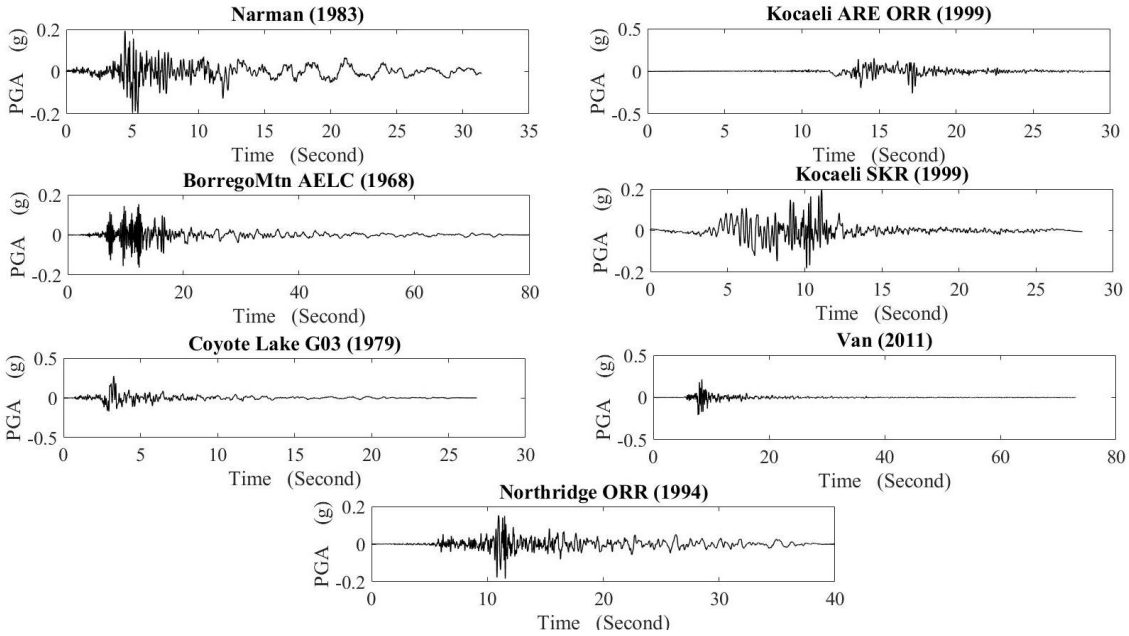

Fig. 10. Matched earthquake record for the 475-year return period.

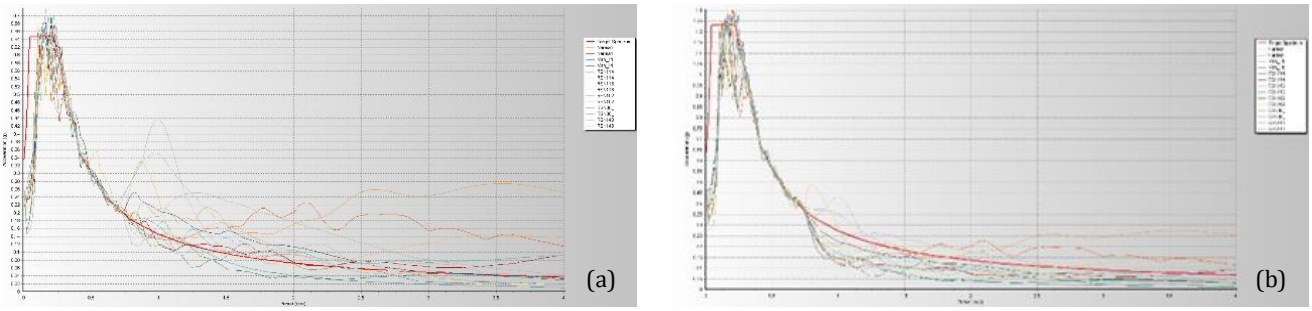

Fig. 11. a) Spectrum acceleration of matched earthquake data and design spectrum for the 475-year return period; b) Spectrum acceleration of matched earthquake data and design spectrum for the 2475-year return period.

Table 3. Column damage limit state.

	Damage State			
	Slight	Moderate	Extensive	Complete
Column Rotation (θ)	θ_y	$2\theta_y$	$4\theta_y$	$8\theta_y$

Table 4 Bearing damage limit state (Nielson, 2005).

	Damage State			
	Slight	Moderate	Extensive	Complete
Pinned Bearing Longitudinal (mm)	28.9	104.2	136.1	186.6
Pinned Bearing Transverse (mm)	28.8	90.9	142.2	195
Sliding Bearing Longitudinal (mm)	28.9	104.2	136.1	186.6
Sliding Bearing Transverse (mm)	28.8	90.9	142.2	195

The yielding rotation of the bridge and column are calculated using Eq (2). Yield rotation for the beam is θ_y=0.01512 for the first and last span and θ_y=0.01827 for the middle spans, and yield rotation for the column is θ_y=0.00414.

$$\theta_y = \frac{W_p F_y I_b}{6EI_b} \quad (2)$$

6.2. Analysis results and discussion

Nonlinear time history analysis was conducted for LL (475-year return period) and UL (2475-year return period) earthquakes. In five of the seven LL earthquake records, the braces were exposed to slight damage; for one LL earthquake, the piers were exposed to collapse damage, for one LL earthquake, the beam was exposed to extensive damage, and for one LL earthquake, sliding bearings were exposed to collapse damage. For seven UL earthquake records, the braces were exposed to slight damage; for three UL earthquakes, the piers were exposed to moderate damage, and for one UL earthquake, the piers were exposed to slight damage. For one UL earthquake, the beams were exposed to extensive damage, and for one UL earthquake, the beams were exposed to slight damage. Two cases of slight, one of moderate and one of extensive damage on the beams, are seen in seven UL earthquake. Tables 5 and 6 show the detailed performance of the bridge components in LL and UL earthquake conditions.

Table 5. Bridge performance for the 475-year return period earthquakes.

	Sliding Bearing	Pinned Bearing	Beam	Pier	Brace
1 Narman (1983)	Collapse	No Damage	Extensive	Collapse	Slight
2 BorregoMtn AELC (1968)	No Damage	No Damage	No Damage	No Damage	No Damage
3 Coyote Lake G03 (1979)	No Damage	No Damage	No Damage	No Damage	Slight
4 Northridge ORR (1994)	No Damage	No Damage	No Damage	No Damage	Slight
5 Kocaeli ARE ORR (1999)	No Damage	No Damage	No Damage	No Damage	No Damage
6 Kocaeli SKR (1999)	No Damage	No Damage	No Damage	No Damage	Slight
7 Van (2011)	No Damage	No Damage	No Damage	No Damage	Slight

Table 6. Bridge performance for the 2475-year return period earthquakes.

	Sliding Bearing	Pinned Bearing	Beam	Pier	Brace
1 Narman (1983)	Slight	No Damage	Extensive	Moderate	Slight
2 BorregoMtn AELC (1968)	No Damage	No Damage	No Damage	No Damage	Slight
3 Coyote Lake G03 (1979)	Extensive	No Damage	Slight	Moderate	Slight
4 Northridge ORR (1994)	Moderate	No Damage	No Damage	Moderate	Slight
5 Kocaeli ARE ORR (1999)	No Damage	No Damage	No Damage	No Damage	Slight
6 Kocaeli SKR (1999)	Slight	No Damage	No Damage	Slight	Slight
7 Van (2011)	No Damage	No Damage	No Damage	No Damage	Slight

Displacement under LL and UL earthquake for longitudinal and transverse directions is calculated using nonlinear time history analysis. Under Narman earthquake conditions, extensive longitudinal deformation is calculated. The mean of LL earthquake longitudinal displacement is 36.4 mm, and without the Narman earthquake, this value decreases to 7.96 mm. The mean value of the LL earthquake transverse direction is calculated as 10.59 mm. The mean values of the UL earthquakes for Longitudinal and Transverse directions are 40.31 mm and 15.34 mm, respectively. These displacements are much smaller than the target displacement calculated using pushover analysis. Fig. 12 shows displacement and intensity measures calculated for LL and UL earthquake records.

Figs. 13 and 14 show the plastic hinge location on the 3D view of the bridge and middle pier hysteretic behavior for LL and UL Narman earthquakes. In the figures, it has been determined that the plastic hinges are intensified at the soil fill boundary of the columns. Soil fill has a great effect on the seismic behavior of the bridge and determines the plastic hinge location. Therefore, bridge performance has varied from the construction date to the present. Time history models solution diverge after extensive plastic deformation at beam elements for both LL and UL Narman earthquakes.

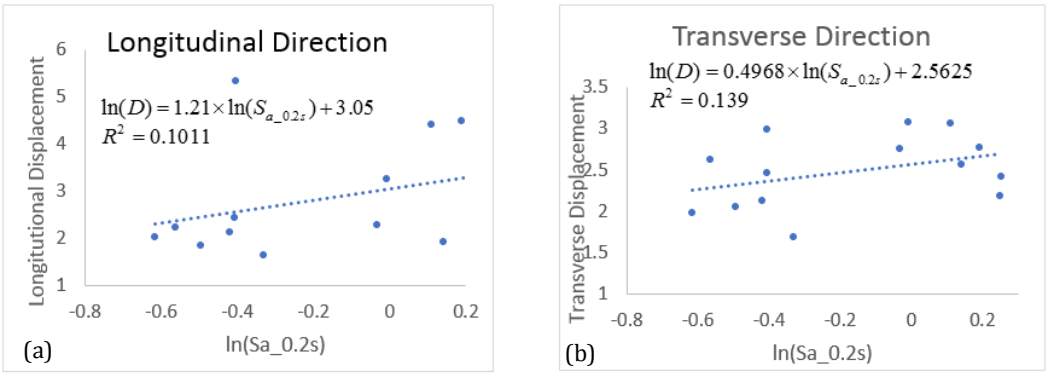

Fig. 12. Displacement and Intensity measure comparison: a) longitudinal direction; b) transverse direction.

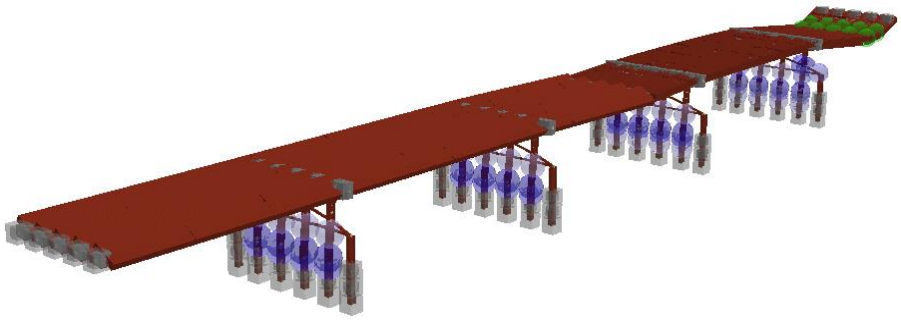

Fig. 13. 3D view of bridge and plastic hinge location for LL Narman earthquake.

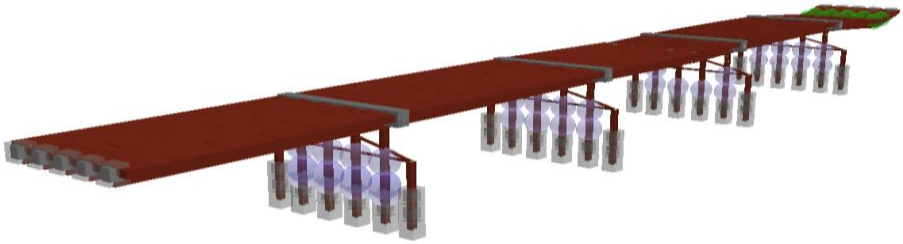

Fig. 14. 3D view of bridge and plastic hinge location for UL Narman earthquake.

7. Conclusions

The finite-element model of the bridge constituted using site investigation and measurement: all the span length and section dimension measured on the bridge. Material properties of the bridge were determined to depend on the construction date of the bridge using past studies in the literature. Modal properties of the bridge calculated using a finite-element model, and modal frequency and modal participation mass ratios were determined. The first mod of the bridge was a longitudinal mod with 0. 49s frequency and represented 55% of the longitudinal mass. The transverse mode frequency was changing between 0.27 s to 0. 33 s and represent 82% of the transverse mass. Finally, the vertical mod frequency calculated as 0.09 s and represent 44% of the vertical mass. Moreover, four different truckloads were applied to the bridge, and maximum moment and vertical displacements were calculated. Maximum moment and displacement visualized under the H20-44 truckload as 41.89 mm and -173.61 kNm, respectively. Vertical displacement limits for the bridge are described as L/800 in ASHTOO bridge design specification. Considering these specifications, the Mahmutcavuş Bridge does not satisfy vertical displacement limits for these four-track loads.

Nonlinear static pushover analysis conducted considering both material nonlinearity and Δ-δ effects. Lateral load acted on the bridge until the top displacement of the middle bridge piers reaches 800 mm in the transverse direction, and plastic hinge formation visualized. The first plastic hinge formed at the brace member, then the next plastic hinge formation started to occur at the bottom of the piers and at the top of the piers. The target displacements for the 2% and 10% possibility, for 50 years period, calculated as 45.36 mm and 22.79 mm, respectively. Finally, the pushover deform shape illustrated to easily calculate the top lateral displacement of all pears.

Seven earthquake records were selected and scaled for 475-year and 2475-year return period earthquake spectrum, which is illustrated by the Turkish Building Seismic Code. Bridge first mod frequency values used to calculate scaling frequency interval. Nonlinear time-history

analyses conducted using scaled earthquake records. Damage states for bridge components determined for bridge piers, beams, brace members, and bearing members. For only one of the seven earthquake record collapse damage visualized for sliding bearing and piers. Only one of the seven earthquakes records extensive damage visualized for the beam members for a scaled earthquake for the 475-year return period. For three of seven earthquakes, moderate damage was visualized for piers for scaled seven earthquake records for the 2475-year return period. For LL earthquake, only one record does not satisfy bridge design specification requirement, and for UL earthquake all the record satisfies bridge design code requirement.

REFERENCES

Atmaca B (2019). Determination of minimum depth of prestressed concrete I-Girder bridge for different design truck. *Computers and Concrete*, 24(4), 303–311.

Bruneau M (1998). Performance of steel bridges during the 1995 Hyogoken – Nanbu (Kobe, Japan) earthquake — a North American perspective. *Engineering Structures*, 20(12), 1063–1078.

Bruneau M, Wilson JC, Tremblay R (1996). Performance of steel bridges during the 1995 Hyogo-ken Nanbu (Kobe, Japan) earthquake. *Canadian Journal of Civil Engineering*, 23(3), 678–713.

Damci E, Temur R, Bekdaş G, Sayin B (2015). Damages and causes on the structures during the October 23, 2011 Van earthquake in Turkey. *Case Studies in Construction Materials*, 3, 112–131.

DesRoches R, Choi E, Leon RT, Dyke SJ, Aschheim M (2004). Seismic response of multiple span steel bridges in central and southeastern United States. I: As built. *Journal of Bridge Engineering*, 9(5), 464–472.

Ghosh J, Padgett JE (2010). Aging considerations in the development of time-dependent seismic fragility curves. *Journal of Structural Engineering*, 136, No. December, 1497–1511.

Inel M, Ozmen HB, Bilgin H (2008). Re-evaluation of building damage during recent earthquakes in Turkey. *Engineering Structures*, 30(2), 412–427.

Kawashima K (2012). Damage of bridges due to the 2011 Great East Japan Earthquake. *Journal of Japan Association for Earthquake Engineering*, 12(4), 319–338.

Korkmaz HH, Korkmaz SZ, Donduren MS (2010). Earthquake hazard and damage on traditional rural structures in Turkey. *Natural Hazards and Earth System Science*, 10(3), 605–622.

Kunnath SK, Erduran A, Chai YH, Yashinsky M (2008). Effect of vertical motions on seismic response of highway bridges. *Journal of Bridge Engineering*, 13(3), 282–290.

Larsson T, Lagerqvist O (2009). Material properties of old steel bridges. *Nordic Steel Construction Conference 2009* (*NSCC2009*), 120–127.

Lu Z, Ge H, Usami T (2004). Applicability of pushover analysis-based seismic performance evaluation procedure for steel arch bridges. *Engineering Structures*, 26(13), 1957–1977.

Nielson BG (2005). Analytical fragility curves for highway bridges in moderate seismic zones. *Georgia Institute of Technology*, No. December, 400.

Nielson BG, DesRoches R (2007). Seismic performance assessment of simply supported and continuous multispan concrete girder highway bridges. *Journal of Bridge Engineering*, 12(5), 611–620.

Padgett JE, DesRoches R (2008). Three-dimensional nonlinear seismic performance evaluation of retrofit measures for typical steel girder bridges. *Engineering Structures*, 30(7), 1869–1878.

Rokneddin K, Ghosh J, Dueñas-Osorio L, Padgett JE (2014). Seismic reliability assessment of aging highway bridge networks with field instrumentation data and correlated failures, II: Application. *Earthquake Spectra*, 30(2), 819–843.

Saadeghvaziri MA, Yazdani-Motlagh AR (2008). Seismic behavior and capacity/demand analyses of three multi-span simply supported bridges. *Engineering Structures*, 30(1), 54–66.

Tolon M, Mızrak KC (2017). Development of disaster management in Turkey: from 1999 Kocaeli Earthquake to 2011 Van Earthquake. *International Journal of Engineering Science and Application*, 1(4), 145–151.

Usami T, Ge H (2009). A performance-based seismic design methodology for steel bridge systems. *Journal of Earthquake and Tsunami*, 3(3), 175–193.

Usami T, Lu Z, Ge H (2005). A seismic upgrading method for steel arch bridges using buckling-restrained braces. *Earthquake Engineering and Structural Dynamics*, 34(4–5), 471–496.

Zheng Y, Usami T, Ge H (2003). Seismic response predictions of multi-span steel bridges through pushover analysis. *Earthquake Engineering and Structural Dynamics*, 32(8), 1259–1274.